ARTICLE

Grafting redox-active molecules on graphene oxide through diamine linker: the length optimization for electron transfer

Rizwan Khan[a,b] and Yuta Nishina[a,b*]

A Redox-active molecule is grafted on graphene oxide (GO) via successive reactions. In the first step, GO is modified with diamine, which acts as linker for the redox-active molecule. In the second step, the redox-active molecule is attached to the amino group of the linker by amide bond formation. Through these processes GO is partially reduced, enhancing its electrochemical properties. The structure of the functionalized GO is characterized by XPS, TGA, FTIR, and CV, and applied for electrodes in supercapacitor (SC). The distance and direction of the redox-active molecule on the electrode affect the SC performance; ethylene diamine is the most promising linker to efficiently transfer electrons from the redox-active molecule to the electrode surface.

Introduction

In the last two decades, graphene has been widely investigated as an electrode material for SCs.[1-4] SCs are electrochemical energy storage devices that assure outstanding power density[5] and cycling stability.[6] SCs can be classified into two types: electric double-layer capacitor (EDLC) and pseudocapacitor. The energy storage mechanism of the EDLC involves a simple charge separation at the interface between the conductive electrode and the electrolyte. EDLC is quite stable, however, specific capacitance is lower than other energy storage systems, such as Li-ion batteries.[7,8] In contrast, specific capacitance of the pseudocapacitor is higher than that of EDLC, but gradually decreases because of the faradic transformation of capacitive electrode materials by gradual degradation.[9] Graphene is a promising electrode component because it has a large surface area,[10–12] excellent electrical conductivity,[13,14] and high mechanical strength.[15,16] For the pseudocapacitive material, redox-active small organic molecules are attractive in terms of structural diversity, ease of synthesis, and handling.[17,18] Combination of graphene and a redox-active molecule is desirable to enhance the overall capacitance and cycling lifetime by taking full advantage of EDLC and pseudocapacitor. Various composites of graphene and redox-active molecules with covalent and non-covalent interactions have been synthesized, and high capacitance has been achieved. The non-covalent interaction between redox-active molecules and graphene is weak and molecular dissociation occurs easily.[19,20] Therefore, in this study, we focused on the covalent bond formation between redox-active molecules and graphene. In the previous researches, catechol,[21] 2-aminoanthraquinone,[22] or

anthraquinone[23,24] was covalently functionalized on graphene without linker molecules. Recently, we reported the covalent functionalization of polymer on graphene via a 1,3-diamino propane linker and achieved stable electrochemical performance.[25] In the previous research, however, the length of the linker molecule was not optimized. In the present study, redox-active molecules were functionalized on graphene through a series of linker molecules by amide bond. The length of the linker molecules was optimized for SC application.

Experimental section

Chemicals and materials

Natural flake graphite was obtained from Bay Carbon Inc. Ethylenediamine, 1,3-diaminopropane, 1,4-diaminobutane, 1,5-diaminopentane, 1,6-diaminohexane, triethylamine, anthraquinone 2-carbonyl chloride were obtained from Tokyo Chemical Industry Co. Ltd. Potassium permanganate ($KMnO_4$), hydrochloric acid (HCl, 36%), sulfuric acid (H_2SO_4, 96%), and dimethylformamide (DMF) were obtained from FUJIFILM Wako Pure Chemical Corporation. All the chemicals were used as received. Graphene oxide (GO) was prepared according to the reported method.[25]

Synthesis of diamine-functionalized GO

Diamine functionalization of GO (**GO 1**) was performed according to our previous report.[25] In a typical procedure, diamine (1 mL) was added dropwise to the suspension of GO (250 mg L^{-1}, 400 mL) under vigorous stirring. The resulting mixture was allowed to stir for 24 h at room temperature, then filtered and thoroughly washed with ethanol and water several times. The obtained solid was freeze-dried for two days.

Grafting redox-active molecule on GO

 Anthraquinone 2-carbonyl chloride (150 mg) was added into a dispersion of **GO 1** (50 mg) in DMF (30 mL), and sonicated for 15 min. Then, triethylamine (400 μL) was added to the mixture. The

a. Graduate school of natural science and technology, Okayama University, 3-1-1 Tsushimanaka, Kita-ku, Okayama 700-8530, Japan
b. Research Core for Interdisciplinary Sciences, Okayama University, 3-1-1 Tsushimanaka, Kita-ku, Okayama 700-8530, Japan

reaction mixture was heated at 80 °C for 24 h, followed by reflux at 180 °C for another 24 h. After completion of the reaction, the reaction mixture was filtered, and the solid product was washed with DMF, aqueous sodium carbonate, and water several times. The prepared material was then dried under vacuum for two days to obtain **GO 2**.

Amide hydrolysis

GO 2a (10 mg) was added to HCl (6M, 20 mL) and sonicated for 30 minutes. Then the suspension was refluxed at 130 °C for 60 h. After completion of the reaction, the reaction mixture was filtered, and the solid product was washed with DMF and water several times and dried under vacuum for 1 day.

Instruments and measurements

The thermogravimetry analysis (TGA, RIGAKU TG 8121) was performed at a heating rate of 10 °C min^{-1} from room temperature to 800 °C under a nitrogen atmosphere. The functional groups were measured by Fourier transform infrared spectrometer (FT-IR, SHIMADZU, IR Tracer 100), using KBr as a binder. The elemental compositions were determined by X-ray photoelectron spectroscopy (XPS). The XPS was carried out on a JPS-9030 with a pass energy of 20 eV. Electrochemical measurements were carried out with an electrochemical working station (Solartron SI1287) at room temperature in a three-electrode cell system. In the three-electrode system, the platinum foil and saturated calomel electrode (SCE) were used as a counter electrode and reference electrode, respectively. The working electrode was fabricated by mixing electrode material (**GO 2**, 4 mg) and carbon black (0.7 mg) in 0.4 mL Nafion solution, which is sonicated for 1 h to make fine dispersion. Then 3 μL of the suspension was dropped onto the glassy carbon electrode (ϕ= 3 mm) using a pipette and dried at 50 °C for 30 min under vacuum. The electrochemical performance was measured under a potential range of -0.5-0.5 V, with a scan rate of 50 mVs^{-1}. All electrochemical experiments were performed in 1 M H_2SO_4 aqueous electrolyte. The specific capacitance (C (F g^{-1})) was calculated from the discharge curve according to the following formula (1).

$$C = (I \cdot \Delta t)/(m \cdot \Delta V) \qquad (1)$$

where I is the constant current in discharging, m is the mass of active material on working electrode, Δt is the discharge time, and ΔV is the voltage change during discharge.
The energy density and power density was calculated according to following formulas (2) and (3).

Energy density (E_d):
$$E_d = (1/2) \, CV^2 \cdot (1/3.6) \qquad (2)$$

Where C is specific capacitance obtained from equation (1) and V is the potential applied.

Power density (P_d):

$$P_d = E_d \cdot (3600/\Delta t) \qquad (3)$$

Where E_d is the energy density obtained from equation (2) and Δt is the discharging time.

Results and Discussion

Our strategy is to functionalize graphene with a redox-active molecule via a linker. The strategy involved two-step reactions: (1) functionalization of graphene with diamine to obtain **GO 1**, (2) addition of anthraquinone moieties to obtain **GO 2** (**Figure 1**). The epoxy ring-opening amination is an established method for the basal plane functionalization of GO.[26–28] Acid chloride can react with the formed amine moiety and latent hydroxy groups on GO (not shown in the figure for simplicity).[29-31]
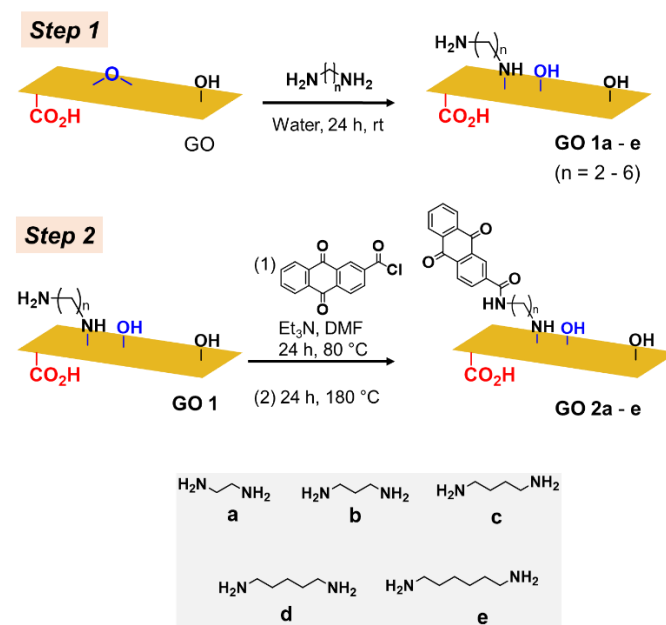

Figure 1. Synthesis route of **GO 2a – e**.

The structure of the materials was confirmed by X-ray photoelectron spectroscopy (XPS), thermogravimetric analysis (TGA), and Fourier-transform infrared (FTIR) spectroscopy.

Initially, the elemental compositions of **GO 1a** and **GO 2a** were analyzed using XPS. XPS spectra of **GO 1a** and **G 2a** showed the presence of nitrogen, which confirmed the functionalization of GO with diamine (**Figure 2ai**).[26,27] Cl was not observed in the XPS spectra of **GO 2a**, meaning that acid chloride was consumed and amide bond was formed between anthraquinone molecule and graphene (**Figure 2aii**). The amount of oxygen in **GO 1a** and **GO 2a** was 25.6%, and 17.1%, respectively (**Table S1**). The smaller amount of oxygen in **GO 2a** suggested a reduction of GO occurred during heating. To gain further insight into the chemical composition, each element was analyzed by narrow-scan XPS. The spectrum of **GO 1a** showed a peak at 399.3 eV at the N 1s region,[26] which suggests the formation of a covalent C–N bond, confirming the functionalization of GO by the amine (**Figure S1a**). The detailed XPS analyses of **GO 1** and **GO 2** are given in the supporting information. Next, the thermal stability of **GO 1a** and **GO 2a** was measured by TGA. The TGA curve of **GO 1a** showed weight loss from 200 °C to 400 °C, which is derived from the thermal decomposition of remaining

oxygenated functional groups and ethylenediamine moiety (**Figure 2bi**).[25,26] In the case of **GO 2a**, a weight loss was observed from 200 °C to 500 °C due to the thermal decomposition of ethylenediamine and anthraquinone molecule (**Figure 2bii**).[32] The lower weight loss observed in **GO 2a** compared with **GO 1a** could be attributed to the reduction of oxygenated functional groups in **GO 2a** during the 2nd step reaction.[33]

The surface functional groups of **GO 1a** and **GO 2a** were further confirmed using FTIR analysis. The FTIR spectrum of **GO 1a** exhibited a peak at 2900 cm^{-1}, attributed to the alkyl chain of ethylenediamine (**Figure 2ci**).[27] A strong peak was observed at 1380 cm^{-1} attributed to C-OH and C-N bond.[34,35] Furthermore, the intensity of the C=O peaks (at 1660 cm^{-1}) was increased in **GO 2a** as compared to **GO 1a**, suggested the attachment of quinone molecules to linker (**Figure 2cii**). All these changes confirmed the formation of the targeted structure of **GO 1a** and **GO 2a**.
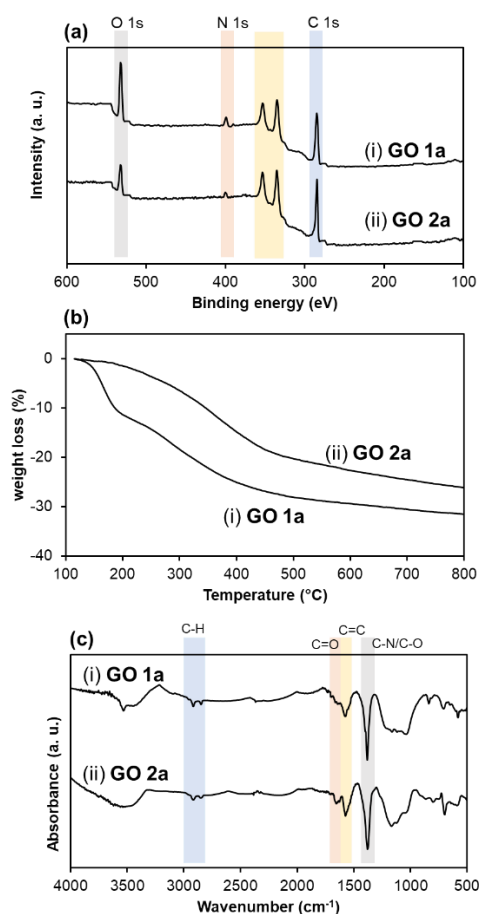

Figure 2. (a) Wide-scan XPS analysis of (i) **GO 1a**, and (ii) **GO 2a**. The yellow band corresponds to signals from gold substrate. (b) thermogravimetric analysis of (i) **GO 1a**, and (ii) **GO 2a**, (c) FTIR analysis of (i) **GO 1a**, and (ii) **GO 2a**.

Optimization of cross-linker for SCs

Next, the linker molecules were optimized for the electron transfer. Initially, the electrochemical behavior of **GO 2** was evaluated by cyclic voltammetry (CV) measurements. The CV curve of **GO 2** showed oxidation and reduction peaks, attributed to the pseudocapacitance behavior of the anthraquinone molecule (**Figure 3a**).[9,36,37] This result confirmed the successful functionalization of graphene with anthraquinone molecule. Afterward, the specific capacitance of all the samples was measured at a current density of 3 A g^{-1}. The capacitance of **GO 2a**, **GO 2b**, **GO 2c**, **GO 2d**, and **GO 2e** was 495 F g^{-1}, 170 F g^{-1}, 180 F g^{-1}, 230 F g^{-1}, and 210 F g^{-1}, respectively (**Figure 3b**). The specific capacitance was calculated from the discharge duration of the galvanostatic charge/discharge curve (**Figure 3c**). **GO 2a** showed the highest capacitance among the others, which may be due to the electronic and steric effects. Electron transfer occurs efficiently from molecule to graphene in a short alkyl chain. Also, the attached molecule may avoid the aggregation of graphene, resulting in a high surface area. A shorter diamine, methylenediamine, might be a more promising linker; however, it can only be available as a salt form. Thus, we decided that ethylenediamine is the most suitable. The specific capacitance was decreased from **GO 2a** to **GO 2b** and irregularly increased and decreased from **GO 2b** to **GO 2e**. When the length of the linker n = 2 and 3, the anthraquinone moiety is perpendicular to the graphene basal plane due to the steric hindrance. In contrast, when n > 4, the linker can be flexible and bent, approaching the anthraquinone to graphene surface and increasing the electron transfer. The longer alkyl chain may increase the flexibility, however, it decreases electron conductivity. Therefore, there is a fine balance between the length of the linker and capacitance. The cycling stability of **GO 2a** was measured at a current density of 10 A g^{-1}. **GO 2a** showed a capacitance retention of 88% after 1500 cycles. Furthermore, the energy density and power density of **GO 2a** was calculated from galvanostatic charge/discharge curve. The energy density and power density of **GO 2a** was 68.7 W h kg^{-1} and 1546.8 W kg^{-1} respectively, at a current density of 3 A g^{-1}.

(a)

(b)

(c)
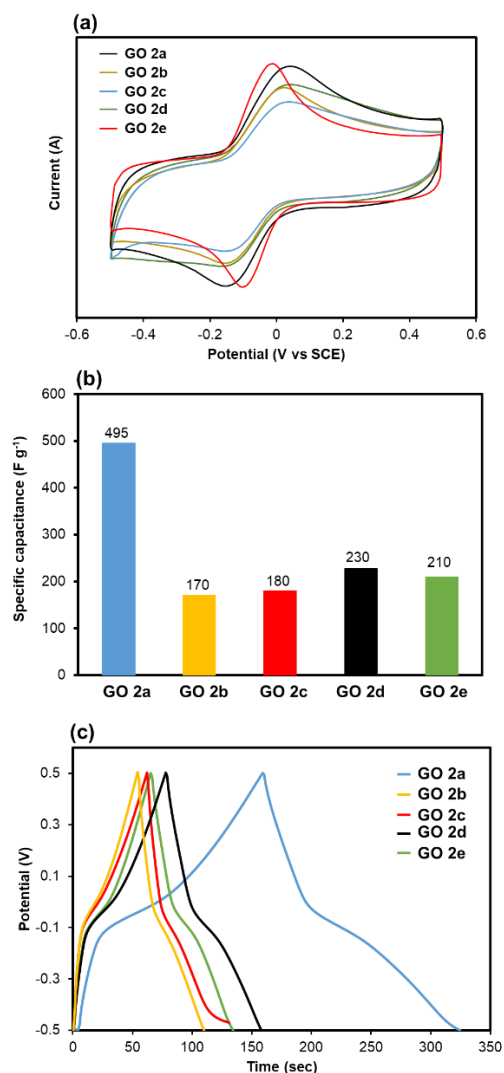
Figure 3. (a) CV of **GO 2a** - **e** at a scan rate of 50 mV s-1, (b) specific capacitance of **GO 2a** - **e** at a current density of 3 A g^{-1} (c) galvanostatic charge/discharge curve of **GO 2a** - **e** at a current density of 3 A g^{-1}.

Detachment of anthraquinone by hydrolysis of the amide bond

GO 2a was heated in an acidic aqueous solution to hydrolyze the amide bond between the linker and anthraquinone molecule (**Figure 4**).[38-41] The phenomenon was confirmed by CV and FTIR analysis. The CV curve of **GO 2a** showed oxidation and reduction peaks at 0.0 V and -0.1V, respectively. In contrast, the hydrolyzed product, **GO 2a$_{hyd}$**, did not show the redox peaks in CV, which suggests the dissociation of anthraquinone moiety from the graphene surface (**Figure S9a**). The hydrolysis reaction was further confirmed by FTIR spectroscopy. A peak at 1726 cm^{-1} was observed in the FTIR spectra of **GO 2a**, assigned to the C=O group of anthraquinone. The peak was disappeared for **GO 2a$_{hyd}$**, suggesting the dissociation of anthraquinone molecules and the reformation of **GO 1a**-like product (**Figure S9b**). These all changes confirmed the hydrolysis of the amide bond between the linker and anthraquinone molecule.[42,43] Although covalent grafting of redox-active molecule via ethylenediamine linker successfully increased the specific capacitance,

degradation in water may be a problem for practical application. Therefore, **GO 2a** would be suitable for a non-aqueous organic type energy storage systems.
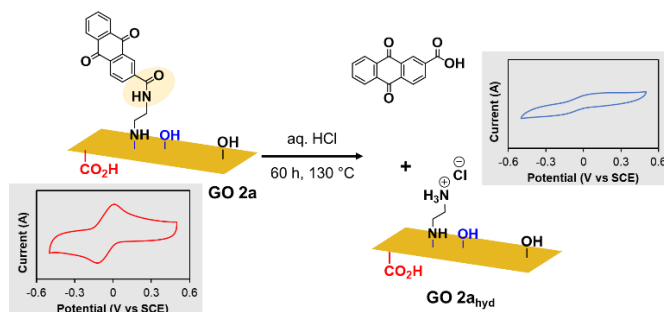

Figure 4. Hydrolysis of **GO 2a**, and corresponding CV curves.

Conclusions

In this work, a redox-active molecule was grafted on GO via a linker. The materials were synthesized through a two-step reaction. In the first step, GO was modified with a diamine. In the second step, the redox-active molecule was attached to the terminal amine of the linker by an amide bond. The structure of the materials was confirmed by various characterization techniques and capacitance was measured to confirm electron transfer. The length of the linker molecules was optimized to achieve high capacitance. Among the linkers with different lengths of alkyl chains, ethylenediamine showed the best performance. This research indicates that a short alkyl chain linker is promising for high SC performance.

Conflicts of interest

There are no conflicts to declare.

Acknowledgements

Notes and references

1. L. L. Zhang, R. Zhou, X. S. Zhao, *J. Mater. Chem.,* 2010, **20**, 5983–5992.
2. C. Liu, Z. Yu, D. Neff, A. Zhamu, B. Z. Jang, *Nano Lett.,* 2010, **10**, 4863–4868.
3. R. Khan, R. Nakagawa, B. Campeon and Y. Nishina, *ACS Appl. Mater. Interfaces*, 2020, **12**, 12736-12742.
4. K. Zhang, L. L. Zhang, X. S. Zhao, J. Wu, *Chem. Mater.,* 2010, **22**, 1392-1401.
5. M. Shanmugavadivel, V.V. Dhayabaran, M. Subramanian, *J. Phys. Chem. Solids,* 2019, **133**, 15–20.
6. Q. Ke, J. Wang, *J. Materiomics.* 2016, **2**, 37–54.
7. S. Ahmed, A. Ahmed, M. Rafat, *J. Saudi Chem. Soc.*, 2018, **22**, 993–1002.
8. W. Ma, S. Chen, S. Yang, M. Zhu, *RSC Adv.*, 2016, **6**, 50112–50118.
9. R. Khan, Y. Nishina, *Nanoscale,* 2021, **13**, 36–50.
10. S. Drieschner, M. Weber, J. Wohlketzetter, J. Vieten, E. Makrygiannis, B.M. Blaschke, V. Morandi, L. Colombo, F. Bonaccorso, J.A. Garrido, *2D Mater.,* 2016, **3**, 045013.

11. A. Klechikov, G. Mercier, T. Sharifi, I. A. Baburin, G. Seifert, A. V. Talyzin, *Chem. Commun.,* 2015, **51**, 15280–15283.
12. Y. Qian, I.M. Ismail, A. Stein, *Carbon*, 2014, **68**, 221–231.
13. H. Murata, Y. Nakajima, N. Saitoh, N. Yoshizawa, T. Suemasu, K. Toko, *Sci. Rep.,* 2019, **9**, 4068.
14. M. A. Worsley, P. J. Pauzauskie, T. Y. Olson, J. Biener, J. H. Satcher, T. F. Baumann, *J. Am. Chem. Soc.*, 2010, **132**, 14067–14069.
15. D. G. Papageorgiou, I. A. Kinloch, R. J. Young, *Prog. Mater. Sci.*, 2017, **90**, 75–127.
16. L. Liu, J. Zhang, J. Zhao, F. Liu, *Nanoscale*, 2012, **4**, 5910–5916.
17. L. Hou, Z. Hu, H. Wu, X. Wang, Y. Xie, S. Li, F. Ma, C. Zhu, *Dalton Trans*., 2019, **48**, 9234–9242.
18. D. M. El-Gendy, N. A. A. Ghany, E. E. F. El Sherbini, N. K. Allam, *Sci. Rep.,* 2017, **7**, 43104.
19. Z. F. Li, H. Zhang, Q. Liu, Y. Liu, L. Stanciu, J. Xie, *Carbon*, 2014, **71**, 257–267.
20. L. Jin, Y. Jiang, M. Zhang, H. Li, L. Xiao, M. Li, Y. Ao, *Sci Rep*., 2018, **8**, 6268.
21. E. Jokar, S. Shahrokhian, A. I. Zad, *Electrochimica Acta*, 2014, **147**, 136–142.
22. Q. Wu, Y. Sun, H. Bai and G. Shi, *Phys. Chem. Chem. Phys.*, 2011, **13**, 11193–11198.
23. B. D. Ossonon and D. Bélanger, *Carbon*, 2017, **111**, 83– 93.
24. M. Mooste, E. K. Põldsepp, B. D. Ossonon, D. Bélanger, K. Tammeveski, *Electrochimica Acta*, 2018, **267**, 246–254.
25. R. Khan and Y. Nishina, *J. Mater. Chem. A*, 2020, **8**, 13718–13724.
26. J. Yan, G. Chen, J. Cao, W. Yang, B. Xie and M. Yang, *New Carbon Mater*., 2012, **27**, 370–376.
27. F. Zhou, H. N. Tien, Q. Dong, W. L. Xu, H. Li, S. Li and M. Yu, *J. Membr. Sci*., 2019, **573**, 184–191.
28. I. A. Vacchi, C. Spinato, J. Raya, A. Bianco and C. Ménard-Moyon, *Nanoscale*, 2016, **8**, 13714–13721.
29. A. Wolk, M. Rosenthal, S. Neuhaus, K. Huber, K. Brassat, J. K. N. Lindner, R. Grothe, G. Grundmeier, W. Bremser and R. Wilhelm, *Sci. Rep*., 2018, **8**, 5843.
30. N. Baig, D. S. Chauhan, T. A. Saleh and M. A. Quraishi, *New J. Chem*., 2019, **43**, 2328–2337.
31. N. A. Kumar, H. J. Choi, Y. R. Shin, D. W. Chang, L. Dai and J. B. Baek, *ACS Nano*, 2012, **6**, 1715–1723.
32. S. B. Sertkol, B. Esat, A. A. Momchilov, M. B. Yilmaz, M. Sertkol, *Carbon*, 2017, **116**, 154-166.
33. W. Chen, L. Yan and P. R. Bangal, *J. Phys. Chem. C*, 2010, **114**, 19885–19890.
34. N. H. Kim, T. Kuila and J. H. Lee, *J. Mater. Chem. A*, 2012, **1**, 1349–1358.
35. Y. Jiang, D. Ni, Q. Ding, B. Chen, X. Chen, Y. Kan and S. Dong, *RSC Adv*., 2018, **8**, 39284-39290.
36. Y. Qin, J. Li, X. Jin, S. Jiao, Y. Chen, W. Cai and R. Cai, *Ceram. Int*., 2020, **46**, 15379-15384.
37. S. T. Senthilkumar, R. K. Selvan and J. S. Melo, *J. Mater. Chem. A*, 2013, **1**, 12386-12394.
38. K. Yates and J. C. Riordan, *Can. J. Chem*., 1965, **43**. DOI:10.1139/v65-314.
39. B. S. Rabinovitch and C. A. Winkler, *Can. J. Res*., 1942, **20**, 73-81.
40. C. Tebes-Stevens, J. M. Patel, W. J. Jones and E. J. Weber, *Environ. Sci. Technol*., 2017, **51**, 5008-5016.
41. R. A. Cox, *Can. J. Chem*., 2005, **83**, 1391-1399.
42. Y. Yan, J. Li, F. Kong, K. Jia, S. He and B. Wang, *Beilstein J. Nanotechnol*., 2017, **8**, 2680–2688.
43. H. Kim and W. J. Kim, *Small*, 2014, **10**, 117–126.